ELSEVIER

Fusion Engineering and Design 27 (1995) 216–225

Fusion Engineering and Design

Analysis of wall-packed–bed thermal interactions

Z.R. Gorbis, M.S. Tillack, F. Tehranian, M.A. Abdou

Mechanical, Aerospace and Nuclear Engineering Department, University of California, Los Angeles, Los Angeles, CA 90024-1597, USA

Abstract

One of the major issues remaining for ceramic breeder blankets involves uncertainties in heat transfer and thermomechanical interactions within the breeder and multiplier regions. Particle bed forms are considered in many reactor blanket designs for both the breeder and Be multiplier. The effective thermal conductivity of beds and the wall–bed thermal conductance are still not adequately characterized, particularly under the influence of mechanical stresses. The problem is particularly serious for the wall conductance between Be and its cladding, where the uncertainty can be greater than 50%. In this work, we describe a new model for the wall–bed conductance that treats the near-wall region as a finite-width zone. The model includes an estimate of the region porosity based on the number of contact points, and the contact area for smooth surfaces. It solves the heat conduction in a near-wall unit cell. The model is verified with existing data and used to predict the range of wall conductances expected in future simulation experiments and in reactor applications.

1. Introduction

Heat transfer in fusion reactor blankets using particle beds depends on both the bulk effective thermal conductivity and the thermal conductance in the near-wall region of the bed. The latter has been studied considerably less than the bulk bed conductivity. Of the theoretical and experimental works [1–14] part of them are related to fusion reactor blanket problems [5–8,10–14]. In almost all the cases, the coefficient of conductance h_w is used, is based on approximation that the thickness of the wall region is zero. But the coefficient h_w is artificial because the porosity and temperature profiles are not constant in the wall region. Most existing models treat only single-size beds and do not include proven recommendations on how to predict the increased porosity of the near-wall region. They often ignore the effect on the conductance of the thermomechanical properties of the wall and the external and internal loading. It was correctly noted in Ref. [13] that no reliable general expression has been developed for the intefacial heat transfer. Some limited number of model predictions and experimental data are available for the wall–bed conductance. The results show substantial variations that it is necessary to explain by both the model assumptions and considerable difficulties to measure h_w. Comparisons of predictions with experimental data in Ref. [7] find that agreement was much poorer for h_w than for the bulk effective conductivity, $k_{eff,b}$. A reasonable agreement ($\pm$ 50%) was obtained with a modified Schlunder correlation related to h_w. The original Schlunder model was found to over-predict measured values, while the Yagi and Kunii model [1] under-predicted (150% low). The Yagi and Kunii model [1] agreed better for the experimental data presented in Ref. [2], but its predictions were close to the lower end

0920-3796/95/$09.50
SSDI 0920-3796(94)00165-0

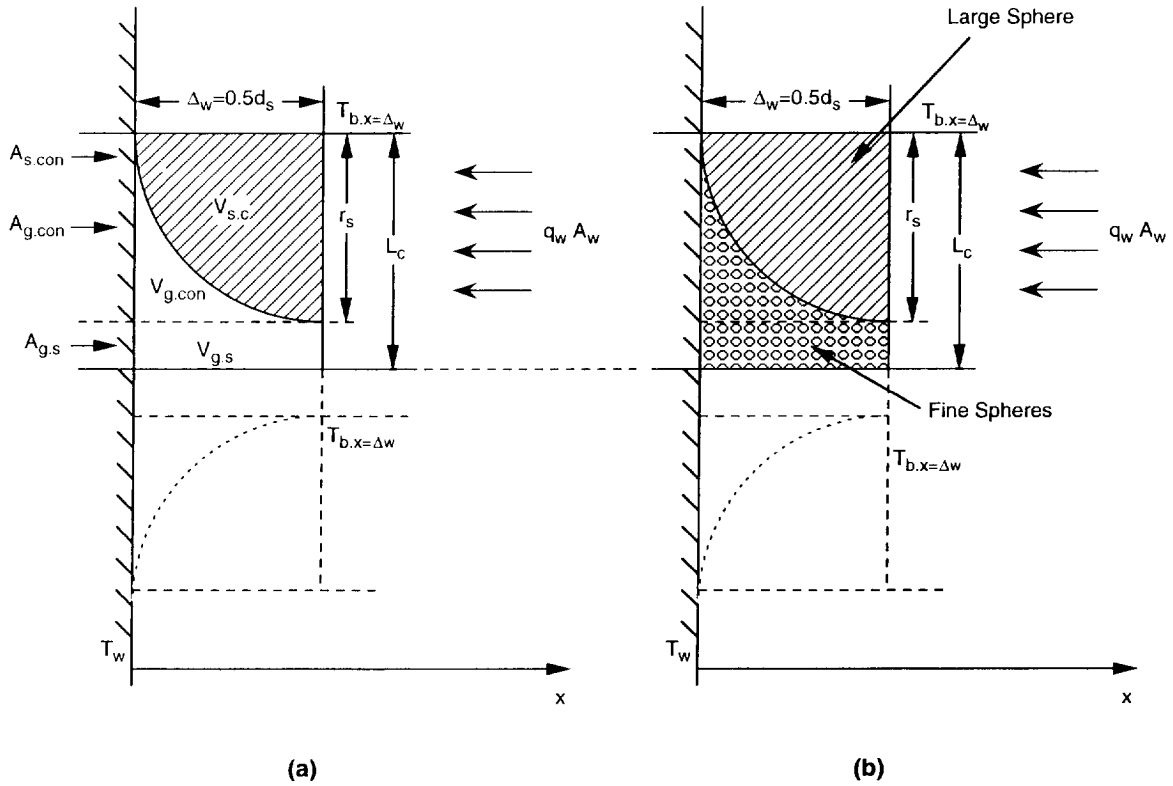

Fig. 1. Representative cell of wall region for (a) single size bed and (b) binary bed.

of the predictions in Ref. [8]. Some experimental data from Refs. [2,5,6] were within the lower and upper limits of the model [8].

A new model has been developed in an attempt to avoid the above mentioned shortages. In this article, model predictions are made and compared with previous studies [4,10,11], which included the effect of external forces on h_w. Comparison between model predictions [1,8] and data [2,5,6] were made in Ref. [12]. This allows application of the model to beryllium and lithium zirconate particle bed with helium cover gas under reactor-relevant conditions. The results of the analyses demonstrate the effect of different types of loadings on the wall region conductance. It is more important for Be than for Li_2ZrO_3 beds, and smaller for binary-size beds than for single-size beds.

2. Description of the model

The model is based on the definition of the real thermal conductance of the wall region with thickness $\Delta_w > 0$:

$$a_{w.b} \equiv \frac{q_w}{(T_{b.x=\Delta} - T_w)} \tag{1}$$

contrary to the usual use of $h_w \equiv q_w/(T_{b.x=0} - T_w)$, where q_w is the heat flux on the wall and $T_{b.x=\Delta}$ and $T_{b.x=0}$ are the temperatures of the bed on the boundaries of the wall region. If $k_{eff.b}$ is the bulk effective conductivity of the bed, and, according to experimental data on porosity distributions, $\Delta_w \cong r_s$, then:

$$\frac{1}{h_w r_s} = \frac{1}{a_{w.b} r_s} - \frac{1}{k_{eff.b}} \tag{2}$$

where r_s is the radius of the particulate and k_g is the gas conductivity. According to Eq. (2), the artificial interface resistance is equal to the real resistance minus the resistance of the bed (which is assumed as uniform in the wall region). But the uniformity changes dramatically exactly in this region, and its porosity $\varepsilon_{w.b}$ reaches a maximum. In the literature, several values for the wall-region porosity can be found. For example,

$\varepsilon_{w.b} = 0.7$ [1], $\varepsilon_{w.b} = 1 - \pi/3\sqrt{3} = 0.4$ [2], or $\varepsilon_{w.b} = 0.55$–0.66, or equal to the mean porosity of the bed ε_b depending on the models used for $\Delta_w = r_s$ [8].

In the proposed model $\varepsilon_{w.b}$ is determined by N_c (the number of particle contact points (per particle) with the wall) which is in all cases equal to one. An expression proposed in Ref. [9], which generalized over analytical and experimental data for local and mean characteristics, gives us $N_c = 19$–$28\ \varepsilon_b$. Using this expression, one may find for $N_c = 1$ that $\varepsilon_{w.b} = 0.643$.

Heat transfer in the representative cell of the model occurs in series through the sphere and sphere–wall contact area, and in parallel through gas parts of the cell (see Fig. 1). Then the dimensionless conductance of a smooth wall-bed interface is defined in general and simplified forms [12]. If $\Delta T_{b.w} \equiv T_{b.x=\Delta} - T_w$ and $\delta_{e.s}$ is the equivalent by volume thickness of the sphere:

$$q_w A_w = a_{w.b} A_w (T_{b.x=\Delta} - T_w) = \frac{A_{con} \Delta T_{b.w}}{\delta_{e.s}/K_s + 1/a_{con}} + A_{g.s} a_{g.s} \Delta T_{b.w} \tag{3}$$

where $A_w \equiv A_{s.con} + A_{g.con} + A_{g.s}$ and $A_{con} \equiv A_{s.con} + A_{g.con}$ represent the surface areas shown in Fig. 1, and:

$$a_{con} = a_{s.con} \frac{A_{s.con}}{A_{con}} + a_{g.con} \frac{A_{g.con}}{A_{con}} \tag{4}$$

$$a_{g.s} = k_g/(\delta_{e.g} + 2j_{g.s}) = k_g/(0.5d_s + 2j_{g.s}) \tag{5}$$

$$\delta_{e.s} = \pi d_s/12 \tag{6}$$

$$A_w = A_{con} + A_{g.s} = A_{s.con} + A_{g.con} + A_{g.s} \tag{7}$$

$$A_w = 0.5 d_s L_c; \quad A_{con} = 0.25 d_s^2; \quad A_{s.con} = 0.5\pi r_{con}^2$$

$$A_{g.con} = 0.25 d_s^2 - \pi r_{con}^2; \quad A_{g.s} = (L_c - 0.5 d_s) 0.5 d_s \tag{8}$$

The half-distance between centers of the wall contacted spheres, L_c, depends on $\varepsilon_{w.b} \equiv V_g/V_c$. Because the volume of gas $V_g = V_{g.con} + V_{g.s}$ and the volume of the cell $V_c = 0.25 d_s^2 L_c$, the porosity of the cell is given by $\varepsilon_{w.b} = 1 - 0.262 d_s/L_c$ or $d_s/L_c = 0.821(1 - \varepsilon_{w.b})$. The conductance of the contact area a_{con} is, according to Eq. (4), the effective conductance because of the existence of two processes: solid (sphere) to solid (wall) contact characterized by the solid contact conductance $a_{s.con}$ and the conductance of gas of contact area $a_{g.con}$.

As was shown in Ref. [4], the contact radius for a spherical particle contacting a flat surface can be defined by an expression based on Hertz's formula for plastic deformations:

$$r_{con} = \sqrt[3]{\frac{3}{4} P r_s \left(\frac{1 - \mu_s^2}{E_s} + \frac{1 - \mu_w^2}{E_w} \right)} \tag{9}$$

where P is the contact load per sphere, r_s is the sphere radius, μ_s and μ_w are the Poisson's ratios for the sphere and wall, E is the modulus of elasticity, and $k_m = 2k_s k_w/(k_s + k_w)$ is the effective thermal conductivity of the contacting surfaces. The contact resistance R_{con} was determined by Yovanovich and Kitscka and shown in Ref. [4] for the simple case where a single spherical surface and flat surface are both smooth and located at the ends of two right circular cylinders as:

$$k_m R_{con} = \left\{ 6 P r_s \left(\frac{1 - \mu_s^2}{E_s} + \frac{1 - \mu_w^2}{E_w} \right) \right\}^{-1/3} \tag{10}$$

By comparing Eqs. (9) and (10), one can find that:

$$k_m R_{con} = \frac{1}{2 r_{con}}; \quad R_{con} = \frac{1}{2 r_{con} k_m} \tag{11}$$

where the unit of R_{con} is K W^{-1}. Applying this result to our model, we may determine the contact conductance in W $(m^2\ K)^{-1}$ as:

$$a_{s.con} = \frac{1}{R_{con} A_{s.con}} = \frac{2 r_{con} k_m}{A_{s.con}} \tag{12}$$

The gas conductance in the contact area $a_{g.con}$ is defined by the equivalent thickness of gas in the contact area $\delta_{e.g.con}$ and the gas temperature jump distance j:

$$a_{g.con} = \frac{k_g}{\delta_{e.g.con} + 2j} = \frac{k_g (1 - 0.5\pi\rho_{con}^2)}{0.477 r_s + 2j} \tag{13}$$

where $\rho_{con} \equiv r_{con}/r_s$ and $\delta_{e.g.con} = V_{g.con}/(A_{con} - A_{s.con}) = 0.0596 d_s^3/(0.25 d_s^2 - 0.5\pi r_{con}^2)$.

According to Eqs. (3)–(8) and (12)–(13), the thermal conductance of the wall–bed interface (in dimensionless form) is:

$$\frac{a_{w.b} r_s}{k_g} = \frac{1.91(1 - \varepsilon_{w.b})}{\dfrac{\pi k_g}{6 k_s} + \dfrac{k_g}{2 k_m \rho_{con} + \dfrac{k_g (1 - 0.5\rho_{con}^2)}{0.477 + 2j/r_s}}} + \frac{1.91\varepsilon_{w.b} - 0.91}{1 + 2j/r_s} \tag{14}$$

Eq. (14) was obtained with the following assumptions [12]:

- the particulates are single-size and spherical;
- free and forced convection of the bed components does not exist or is negligible;
- thermal radiation is negligible;
- only elastic deformation is considered; for other conditions, Eq. (9) must be corrected;
- the porosity distribution is independent of loading after the bed is packed.

Table 1
Characteristics of studies

Study	Type of bed	Components of the bed	Mean bed temp. (°C)	Max σ_{ext} (Pa)	Ratio $(H/D)_b$	$\sigma_{ext.w}$ (Pa)	Source of external load
k_{eff}, h_w (fusion relevant conditions) [14]	Single-size, binary-size; $d_s = 2$ and 1.2 mm	Be, Li_2ZrO_3 in He	325, 500	10^6	0.125	$=\sigma_{ext}$	pressure of coolant, thermal stresses
k_{eff}, h_w [10,11]	Single-size, $d_s = 0.8$; 1.2; 2 mm	Al and Be in air and He; Li_2ZrO_3 in air	29–31 70	1.4×10^6 1.2×10^6	3.25	$<\sigma_{ext}$	Hydraulic press
$a_{w.b}$ in vacuum [4]	Single-size; $d_s = 2.38$ mm	Al, Brass Chromium Alloy, SS	Interface temperature 66	Apparent pressure 7.5×10^6	$\lesssim 2$	$\cong\sigma_{ext}$	Screw jack

If the Knudsen number of the contact area and gas layer between spheres in contact with the wall is less than 0.001, then the Smoluchovskii effect can be neglected and the gas may be considered a continuous medium. This condition is often applicable when the pressure of the gas in the bed is not less than 1 atm. Because of the small value of ρ_{con}, the quantity $0.5\rho_{con}^2$ is very often $\ll 1$ and can be neglected. The analysis here assumes smooth particulates and wall. But, if it is necessary, the thermal radiation, roughness and Smoluchovskii effects can be in the proposed model of the wall region. Taking into consideration that $j \to 0$ and $\rho_{con}^2 \ll 1$, Eq. (14) may be simplified for low ratio k_g/k_s and $\varepsilon_{w.b} = 0.643$ as follows:

$$a_{w.b} r_s/k_g = 0.682(2k_m\rho_{con}/k_g + 2.09) + 0.318 \quad (15)$$

and for binary beds:

$$\frac{a_{w.b} r_s}{k_g} = 0.682\left(2\frac{k_m}{k_g}\rho_{con} + 2.09\frac{k_{eff.f}}{k_g}\right) + 0.318\frac{k_{eff.f}}{k_g} \quad (16)$$

where $k_m \equiv 2k_s k_w/(k_s + k_w)$; k_g, k_s, and k_w are effective, gas, sphere and wall conductivities; $\rho_{con} \equiv r_{con}/r_s$ is the dimensionless contact radius; and $k_{eff.f}$ is the fine particulates effective conductivity in the wall region. As was shown by Ref. [12]:

$$r_{con}^3 - Br_{con}^2 - C = 0 \quad (17)$$

where B and C are complexes depending on the type of stresses existing in the wall region of the bed. Then

$$\rho_{con}^3 - B^*\rho_{con}^2 - C^* = 0 \quad (18)$$

$$B^* \cong 0.785\alpha_v \Delta T_{i.w} \frac{1-\mu_s^2}{1-2\mu_s}\left(1 + \frac{1-\mu_w^2}{1-\mu_s^2}\frac{E_s}{E_w}\right)\frac{\varepsilon_b}{\varepsilon_{w.b}} \quad (19)$$

$$C^* \cong 2.355\sigma_{ext.w}\frac{1-\mu_s^2}{E_s}\left(1 + \frac{1-\mu_w^2}{1-\mu_s^2}\frac{E_s}{E_w}\right) \quad (20)$$

where $\alpha_v \equiv$ mean coefficient of the sphere volume thermal expansion; $\Delta T_{i.w} \equiv T_{w.b} - T_o$; $T_{w.b}$, T_o are the steady state and inital temperatures of the region; E_s, E_w are the sphere and wall Young's modulus; and $\sigma_{ext.w}$ is the external pressure applied to the contact wall.

Three main scenarios are considered:

(1) thermal expansion prevails, and the clad boundary conditions are rigid. In accordance with Eqs. (20) and (18):

$$C^* = 0; \quad \rho_{con} = B^* \quad (21)$$

(2) external loading prevails, walls are flexible and according to Eqs. (19) and (18):

$$B^* = 0; \quad \rho_{con} = \sqrt[3]{C^*} \quad (22)$$

(3) a combination of internal and external loading exists; it has to be analyzed by Eqs. (18)–(20).

In some experimental studies the external pressure σ_{ext} is applied away from the contact wall which is used for the measurement of $a_{w.b}$ [4,10,11]. In this case $\sigma_{ext.w} < \sigma_{ext}$ because, in general, stresses fade exponentially into the bed. But for "short" beds the stress field is close to a linear distribution, depending on the ratio of thickness (in the loading direction) to width of the bed $(H/D)_b$. If $(H/D)_b \leqslant 2$, $\sigma_{ext.w} \cong \sigma_{ext}$, but for $(H/D)_b > 2$ one can assume that $\sigma_{ext.w} \cong \sigma_{ext}(D/H)_b$.

Table 2
Properties of materials used in the analysis

	SS	Be	Li_2ZrO_3	Al	Brass	Chromium alloy
k (W (m^2 K)$^{-1}$)	17.3	190	~5	205 [10] 121.3 [4]	117.8	44.8
E (10^{10} Pa)	19	29	20.3	6.9 [10] 7.2 [4]	10.5	19.7
μ	0.27	0.07	0.2	0.34	~0.3	~0.27
α_v (10^{-6} K^{-1})	54	42 (200°C) 46 (400°C)	30	69	57	~54

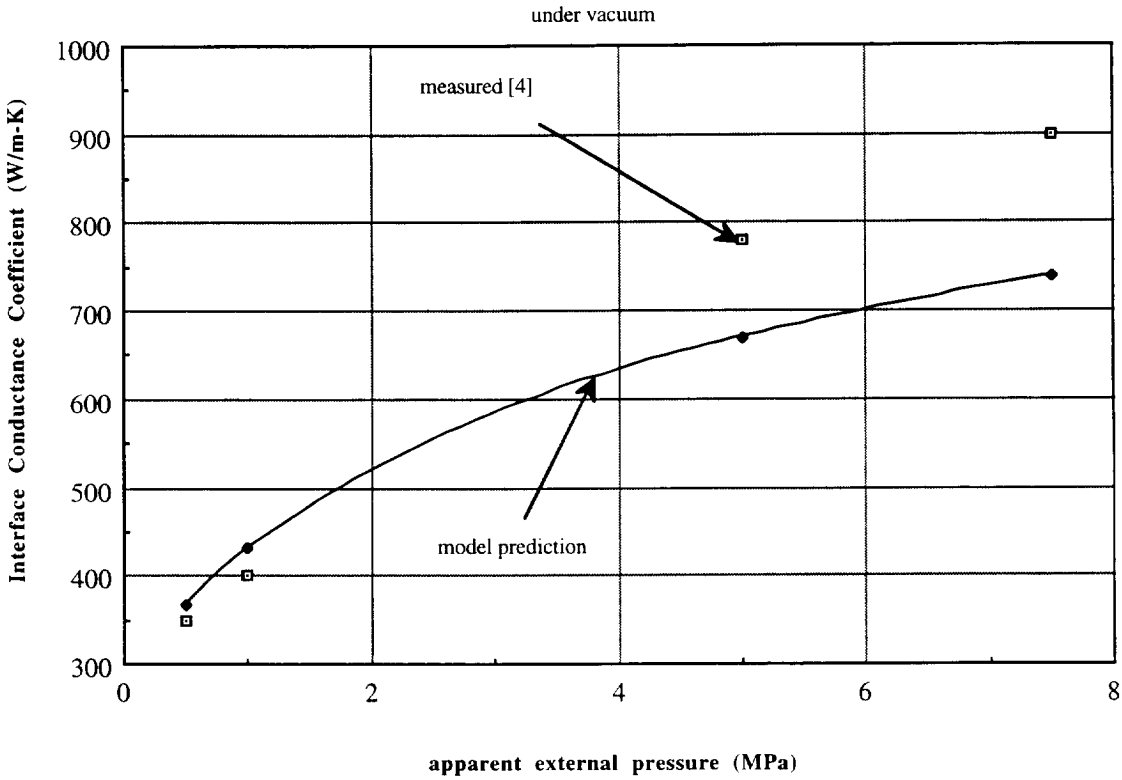

Fig. 2. Aluminum particle bed/stainless steel interface conductance coefficient as a function of the apparent external pressure.

3. Comparison with experimental data

Data of studies detailed in Refs. [4,10,11,14] are used because they deal with the effect of outside pressure on h_w. Some characteristics of them are shown in Tables 1 and 2.

In Ref. [4], the apparent external pressure $\sigma_{ext.ap}$ must refer to the contacted wall spheres and this is why $\sigma_{ext} > \sigma_{ext.ap}$ depending on the number of spheres. Because of the vacuum, $a_g = 0$ and $a_{w.b}$ is the solid–solid contact conductance; $a_{w.con} = 2\rho_{con}k_m/r_s$. Some results of the comparison with data from Ref. [4] are shown in

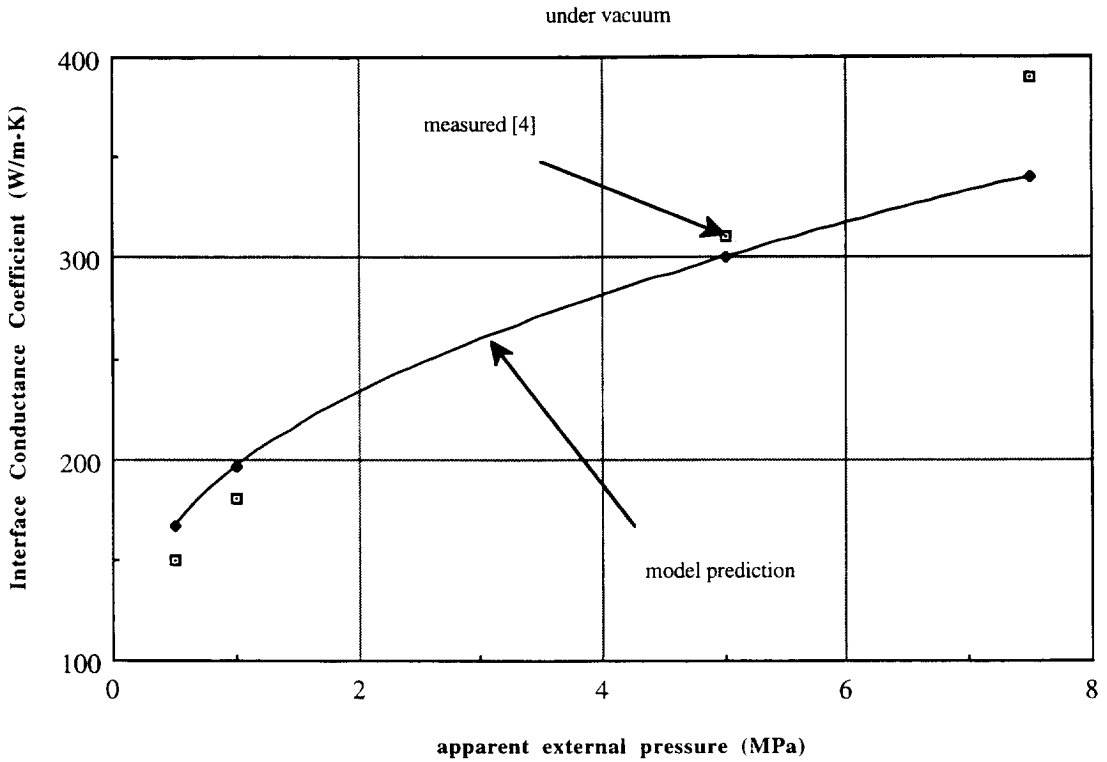

Fig. 3. SS-304 particle bed/stainless steel interface conductance coefficient as a function of apparent pressure.

Figs. 2 and 3 for aluminum and steel spheres, which represent a wide range of sphere conductivity. The wall material in all cases is stainless steel. In this case, the main contribution can come from both external and internal loading because of their relatively low values. The dimensionless contact radius is calculated by Eqs. (18)–(20). It is changed from 6.8×10^{-3} to 1.4×10^{-2} for Al spheres, and from 5.8×10^{-3} to 1.15×10^{-2} for SS-304 spheres when $\sigma_{ext.w}$ is 2.65×10^{4}–4×10^{5} Pa. According to Figs. 2 and 3, there is good agreement between experimental and predicted data. In both cases, the increase of outside pressure 15 times from the minimum to the maximum with constant thermal stress, σ_{th}, leads to more than double the conductance growth. Comparisons for intermediate conductivity spheres (brass and chromium alloy) showed similar good agreement. The maximum/minimum differences between predicted and measured values of $a_{w.con}$ were about $-20\%/+13\%$ and they occured under maximum/minimum pressure (Figs. 2 and 3). The possible reason for this trend is the approximate equality of $\sigma_{ext.w}$ and σ_{ext} (Table 1). Notice that effect of external loading on $a_{w.b}$ will be smaller than on $a_{w.con}$ when there is background gas, because a_g does not depend on σ_{ext}.

Comparisons with experimental data taken from Refs. [10] and [11] are summarized in Table 3. In this case, the external pressure prevails and the dimensionless contact radius is calculated by Eqs. (20) and (22) where $\sigma_{ext.w} = \sigma_{ext}(D/H)_b = 0.308\sigma_{ext}$. The experimental $a_{w.b}$ is found by Eq. (2) using experimental data on h_w and $k_{eff.b}$. The predicted $a_{w.b}$ is calculated by Eq. (15) with correction to the sphere thermal resistance $\pi k_g/6k_s$ [12] for ceramic particulates. As shown in Fig. 4, the results of the comparison are in reasonable agreement for the Al/air bed. For other types of beds they show differences in values, but the same trend of the effect of external pressure on conductance when σ_{ext} increases from the minimum 0.22×10^{6} Pa to the maximum 1×10^{6} Pa. For Li_2ZrO_3 the loading has practically no effect on $a_{w.b}$ because of the relatively small ceramic thermal conductivity and small contribution of $a_{w.con}$ on $a_{w.b}$ (especially for the He bed). For metal particulates the trend is similar for the expected and measured $a_{w.b}$ (they are increasing by the increased effect of

Table 3
Comparison of experimental [10,11] and predicted data on $a_{w.b}$ ($p_g = 1$ atm)

	Al/Air, $d_s = 0.8$ mm		Al/He, $d_s = 0.8$ mm		Be/He, $d_s = 2$ mm	
External pressure σ_{ext} (10^6 Pa)	Experiment $h_w/a_{w.b}$	Prediction $a_{w.b}$	Experiment $h_w/a_{w.b}$	Prediction $a_{w.b}$	Experiment $h_{w.b}/a_{w.b}$	Prediction $a_{w.b}$
0.22	1460/1010	1700	6800/4650	2300	absent	744
0.55	1900/1510	2300	8500/5790	2850	absent	920
1.0	2300/1870	2800	8500/6030	3300	absent	1060
	Li_2ZrO_3/Air, $d_s = 1.2$ mm		Li_2ZrO_3/He, $d_s = 1.2$ mm			
	Experiment $h_w/a_{w.b}$	Prediction $a_{w.b}$	Experiment $h_w/a_{w.b}$	Prediction $a_{w.b}$		
0.22	130/122	283	180/166	693		
0.55	150/140	356	180/166	728		
1.0	150/141	415	180/166	780		

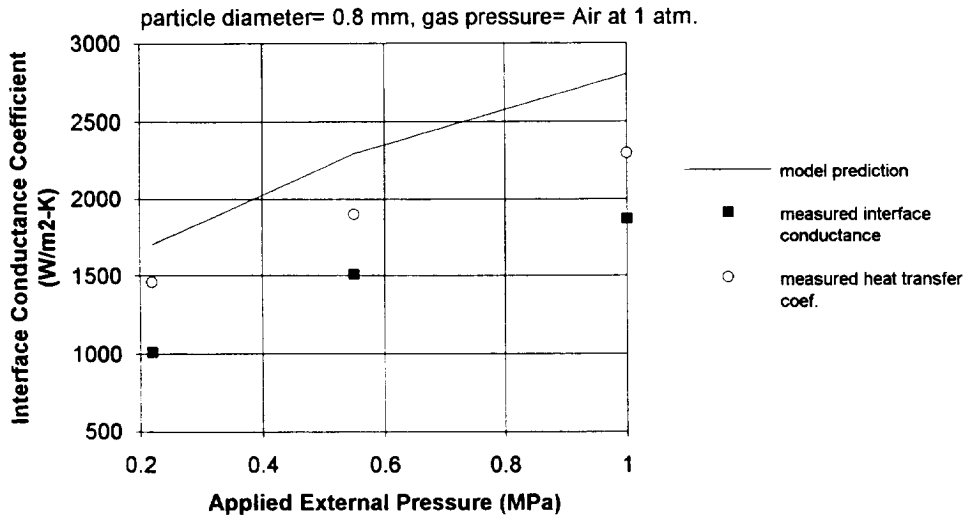

Fig. 4. Aluminum particle bed/stainless steel wall interface conductance coefficient.

loading on $a_{w.con}$). But the values of measured thermal conductance shown in Table 3 are different than the model predictions (particularly for the He beds) up to by a factor of approximately 3–4 for Li_2ZrO_3–He bed. These discrepancies are believed to be a result of the experimental uncertainties involved in the measured quantities such as the heat flux, interface temperatures, bed thickness, etc. In the case of Li_2ZrO_3–He beds, experimental uncertainties only in $k_{eff.b}$ were up to 100%.

The model predictions were compared with other experimental data for He beds in Ref. [12]. The differences with $a_{w.b}$ measured in Ref. [4] for glass–He beds were approximately 28% and with h_w measured in Ref. [6] for outer wall of the Al–He beds are from 13.7% to 45.6%.

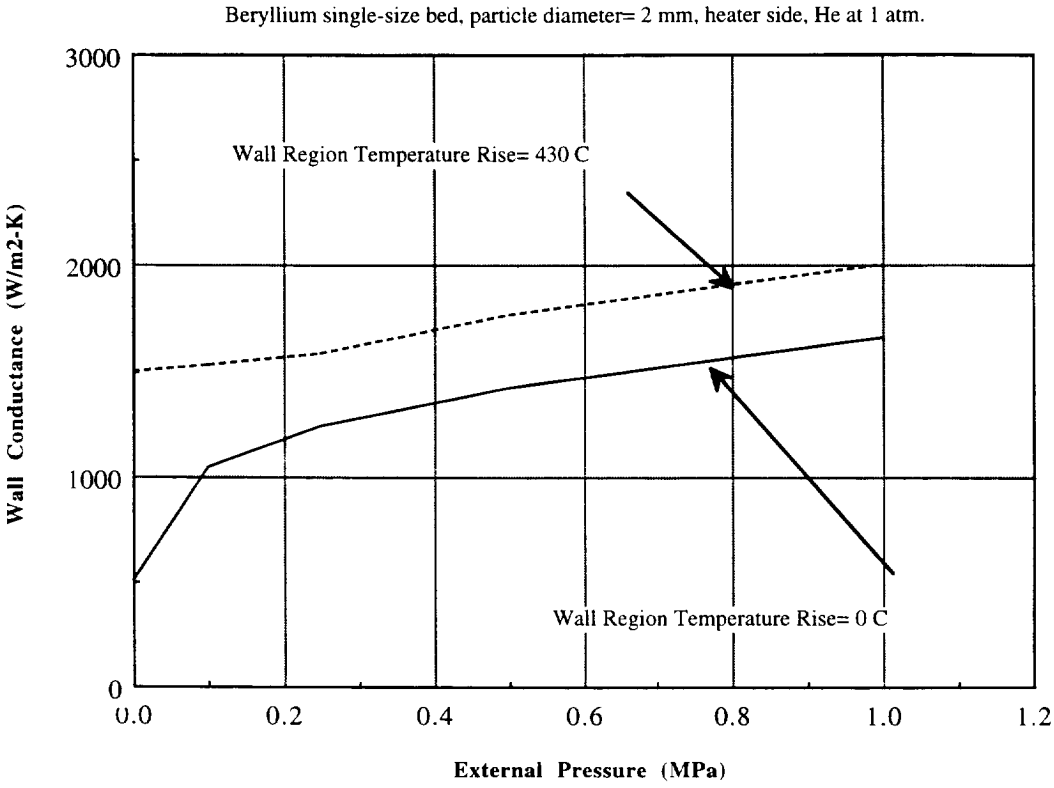

Fig. 5. Predicted values of the wall conductance under reactor operating conditions.

4. Predictions of interface conductance for reactor conditions

Next, the analysis of $a_{w.b}$ is made for cooled and heated sides of beryllium and lithium zirconate beds with porosity 0.35 (single-size beds) and 0.14 (Be binary bed), for rigid and flexible (from the coolant side) boundary conditions and maximum temperature 450 and 685°C of Be and Li_2ZrO_3 beds respectively. For rigid walls, σ_{ext} is assumed zero and only thermal stresses may occur if $\Delta T_{i.w} > 0$ (gravity effect may be neglected). External loading by flexible walls can have an effect on $a_{w.b}$ separately if $\Delta T_{i.w} = 0$, or in combination with thermal expansion. The main results of consideration of these three main scenarios of possible stresses are presented in Figs. 5–8. According to the figures, the effect of internal (thermal) expansion may not be ignored for single-size beds, especially for fixed clads ($\sigma_{ext} = 0$). This effect is more important for Be than for Li_2ZrO_3 beds.

For binary beds, $a_{w.b}$ often depends on an increase of the conductivity of the gas areas filled with fine particulates which do not contact the wall. By analyses of Eq. (16) one may obtain that the effect of loading can be ignored if $k_{eff.f} \gtrsim 3.13 k_m \rho_{con}$. Then $a_{w.b} \cong 1.74 k_{eff.f}/r_s$ [12]. The Be binary bed's conductance with rigid walls is estimated as 1600 and 3100 $W(m^2 K)^{-1}$ for cooled and heated sides. It is about twice as much as for single-size beds. But in all cases, the effect of loading (including σ_{ext}) on ρ_{con} and $a_{w.b}$ is much smaller than for single-size beds.

According the the figures, if the clad is flexible and only external loading is applied, increasing the pressure from 0.1 to 1 MPa increases the thermal conductance coefficient by 60%–70% for Be and 20%–28% for Li_2ZrO_3 beds. The conductance will be minimum, and depend paractically only on gas area conductance, if both external and internal loading are absent.

Under a combination of both internal and external loads, increasing the external pressure from zero (ther-

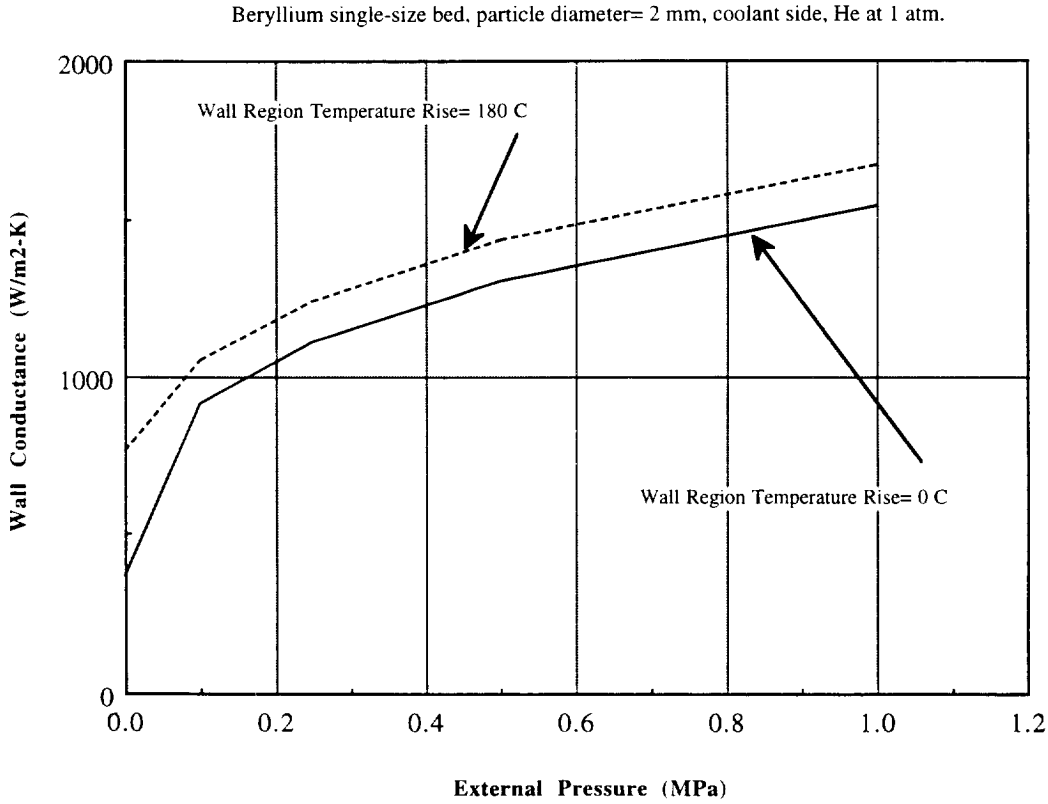

Fig. 6. Predicted values of the wall conductance under reactor operating conditions.

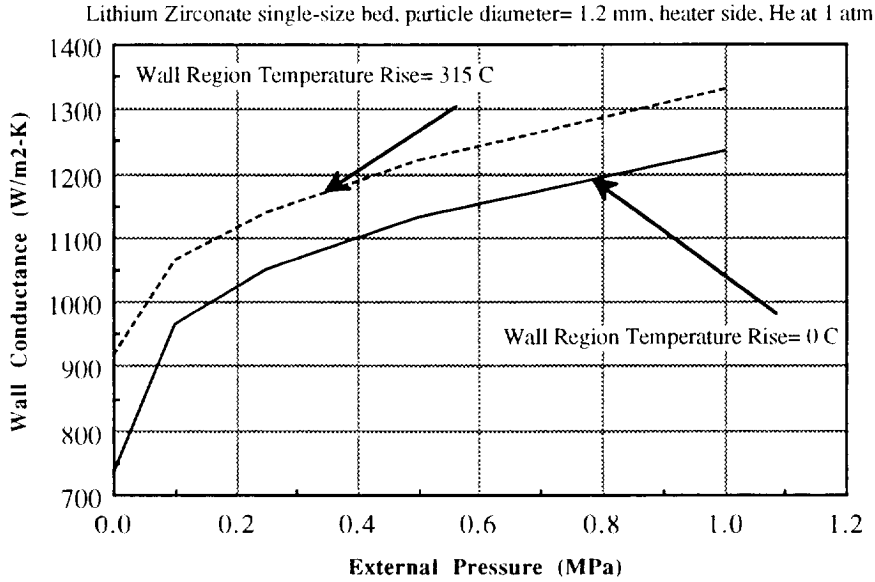

Fig. 7. Predicted values of the wall conductance under reactor operating conditions.

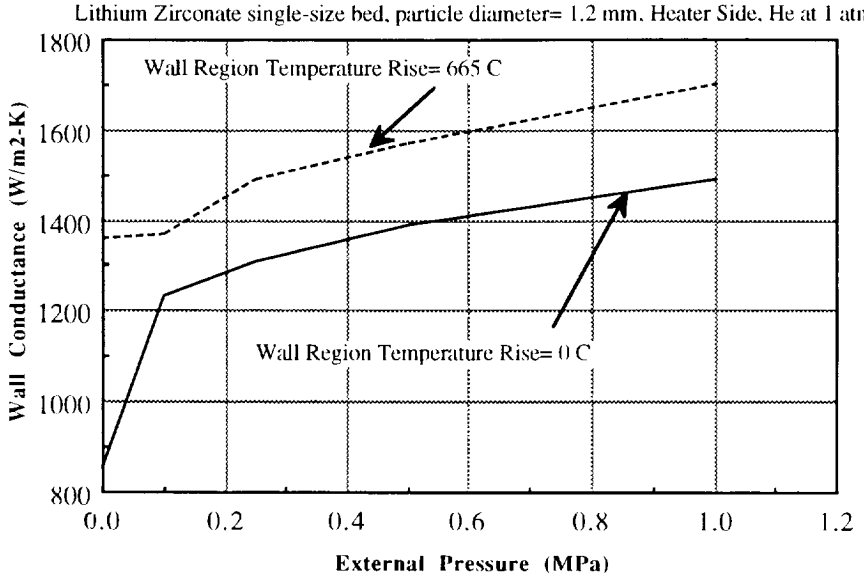

Fig. 8. Predicted values of the wall conductance under reactor operating conditions.

mal expansion only) to 1 MPa results in an increase of conductance of ~200% for the coolant side and to ~34% for the heated side of the Be bed under full power and temperature levels in the bed. The effect of combined loads is smaller for Li_2ZrO_3 beds: 45% and 25% respectively, which can be close to uncertainty range of the model.

Future analysis is planned for cyclic loading, including transient conditions, and for heat transfer through the core of the beds under different types of loading.

References

[1] S. Yagi and D. Kunii, Heat transfer in packed beds, in International Development in Heat Transfer, Part IV, 1962, 750–756.

[2] K. Ofuchi and D. Kunii, Heat transfer characteristics of packed beds with stagnant fluids, Int. Heat Mass Transfer 8 (1965) 749–757.

[3] W.W. Kitsha and M.M. Yovanovich, Experimental investigation on the overall thermal resistance of sphere-flat contacts, in M.M. Ivanovich (ed.), AIAA Progress in Astronautics and Aeromatics, Vol. 39, MIT Press, Cambridge, MA, 1975, pp. 93–110.

[4] G.P. Peterson and L.S. Fletcher, Thermal contact conductance of packed beds on contact with a flat surface, J. heat Transfer 110 (February 1988) 38–41.

[5] M.S. Tillack et al., Experimental studies of active temperature control in solid breeder blankets, Fusion Engineering and Design 17 (1991) 165–170.

[6] M. Dalle Donne and G. Gordon, Heat transfer in pebble beds for fusion blankets, Fusion Technology 17 (July 1990) 597–635.

[7] W. Fundamenski and P. Gierszewski, Heat transfer correlations for packed beds, Fusion Technology 21 (May 1992) 2123–2127.

[8] A.R. Raffay, Packed bed conductance, UCLA-FNT-58, UCLA-ENG-93-01 (July 1992) 1–14.

[9] M.E. Aerov and O.M. Todes, Apparatus with stationary granular bed, Chemistry, Leningrad, 1979 (in Russian).

[10] F. Tehranian, Effect of external load on particle beds thermal properties, UCLA-FNT-68, ENG-93-24 (May 1993).

[11] F. Tehranian and M.A. Abdou, Experimental study of the effect of external pressure on particle bed effective properties, submitted to Fusion Technology (November 1993).

[12] Z.R. Gorbis, Novel model of wall-packed bed thermal interaction, UCLA-FNT-71, ENG-93-81 (August 1993) 1–26.

[13] K.E. Kasza, ANL ITER high-heat-flux blanket module heat transfer experiments, ANL-FPP-TM-262 (February 1992).

[14] M.S. Tillack, Description of small scale solid breeder blanket simulation experiment–HiTeC, UCLA-IFNT-10 (May 1993).